

# Mechanical Performance Analysis and Experimental Research on High-Pressure Swing Components Assembled in Swing-After-the-Pump Rocket Engine

Yuting Zhou<sup>1,\*</sup>, Zhenzhong Zhang<sup>2</sup> and Zhaoyu Liu<sup>3</sup>

<sup>1</sup> Beijing Aerospace Propulsion Institute, Beijing, China, \*zhouyuting@buaa.edu.cn; <sup>2</sup> Beijing Aerospace Propulsion Institute, Beijing, China; <sup>3</sup> Beijing Aerospace Propulsion Institute, Beijing, China

**Abstract:** This paper, based on a combination of numerical analysis and experimental testing methods, conducts a mechanical performance analysis and experimental research on a High- Pressure Swing Component for a Swing-After-the-Pump rocket engine. Taking into account the nonlinearities due to material properties, geometric configurations, and boundary conditions, the paper establishes a numerical analysis model for the High-Pressure Swing Component to study its mechanical characteristics. The fatigue life of the High-Pressure Swing Component is assessed using a strain-corrected Manson-Coffin formula. On this basis, a high-pressure swing test is conducted to effectively simulate actual working boundaries and load conditions, and to perform fatigue life testing. By comparing numerical simulation results with experimental data, the validity of the finite element simulation is verified. Additionally, the actual oscillating torque is obtained and the product's fatigue life is evaluated, providing significant experimental data for the development of the Swing-After-the-Pump rocket engine.

**Keywords:** High-pressure swing component; Swing-After-the-Pump; Rocket engine; Manson-Coffin formula

## 1 Introduction

Swing-After-the-Pump (SAP) technology is one of the key technologies in the development of liquid rocket engines. It can effectively reduce the swing mass of the engine, lower the swing torque, and greatly improve the swing characteristics of the engine system. The core of this technology lies in the design and experimental verification of the High-Pressure Swing Component (HPS(c)). There has been significant development in SAP research abroad, with Russian high-pressure staged combustion engines such as RD-170, RD-180, and RD-191 utilizing SAP technology. To achieve the objectives of manned lunar landings and other space engineering projects, China has also developed some high- thrust liquid-oxygen/kerosene rocket engines based on the SAP technology [2]. In recent years, many commercial aerospace companies have also begun to develop reusable SAP engines, considering cost and technical maturity. In summary, the research and design of the HPSC stand as the cornerstone for advancing the SAP engine.

Several technical difficulties arise in the development of swing devices: Firstly, the design of swing component involves various types and functions, which requires in-depth analysis and comparison of characteristics of each type, combined with the actual needs of the pipeline, to determine the design scheme [5,8,9]. The design of bellows needs to overcome the harsh working conditions of high pressure and achieve the required angle compensation, which presents considerable challenges. Secondly, the external load-bearing structure is the

main load-bearing component. Due to the large pressure that generates a separating force, and the increased force transmission path brought by large diameters, the resulting bending moments put the material under a combined state of tensile and bending stress, with stress values far exceeding the strength limit <sup>[3,10]</sup>.

Within the scope of literature known to the authors, there are currently very few studies on the overall design analysis and testing of the swing component in the SAP engine. Most studies focus on the analysis of the mechanical characteristics of the bellows in the swing component. Research on multi-layered bellows structures has been conducted extensively both domestically and internationally. For example, Anderson <sup>[1]</sup> designed U-shaped and reinforced bellows considering single-layer bellows as independent parts without interaction. Hulbert <sup>[7]</sup> and others used equivalent reduced models to replace multi-layered bellows, adjusting the modulus of elasticity to simulate the interlayer contact of multiple layers. Their conclusions indicate that the simplification method of the equivalent model is very complex and uncertain. Research by Asyem <sup>[6]</sup> at Xinjiang University and others analyzed the impact of the design parameters of bellows on their performance. Lang <sup>[4]</sup> from Dalian University of Technology and collaborators conducted a finite element analysis on the bending stress of bellows. Most relevant studies lack of experiments data to verify simulation results.

Therefore in this article, we demonstrate a comprehensive methodology for analyzing and testing the mechanical performance of the HPSC. The main contribution of the paper is listed in follows:

(a) A numerical model is created to accurately represent the mechanical behavior of the High-Pressure Swing Component, taking into consideration the complex nonlinear effects arising from the material characteristics, shape of the component, and imposed boundary conditions.

(b) We executed a series of high-pressure experimental tests that closely replicated the actual working conditions of the engine component to directly assess its fatigue life under realistic load circumstances.

(c) By contrasting the numerical simulation results against the empirical data gathered from high-pressure testing, the research confirmed the numerical model’s predictions and provided crucial insights into the component’s operational durability, which will support the advancement of SAP rocket engines.

## 2 Finite Element Model Description

### 2.1 Model Parameters

This paper takes the HPSC of the SAP engine as the research subject, and studies its mechanical performance and fatigue life. The HPSC is an important component of the engine’s oscillating mechanism, with capabilities such as conical swinging, withstanding high pressures, and transporting mediums. It consists of a bellows and a load-bearing structure, as shown in Figure 1. The load-bearing structure is composed of a common flat ring, upper and lower force-transmitting fork rings, a deflector sleeve, bearings, pins, and a shaft sleeve, primarily made of GH4169 material. And its mechanical properties of the material are displayed in Table 1.

Table 1 Mechanical properties of the material.

Material	Temperature	EM1	PR2	SE3	Yield limit	PEF4	Density
06Cr18Ni11Ti	25°C	195GPa	0.3	520MPa	205MPa	> 40%	7830kg/m <sup>3</sup>
GH4169	25°C	204GPa	0.3	1240MPa	1040MPa	> 12%	8240kg/m <sup>3</sup>

1 Elasticity Modulus; 2 Poisson’s Ratio; 3 Strength of Extension; 4 Percentage Elongation after Fracture.

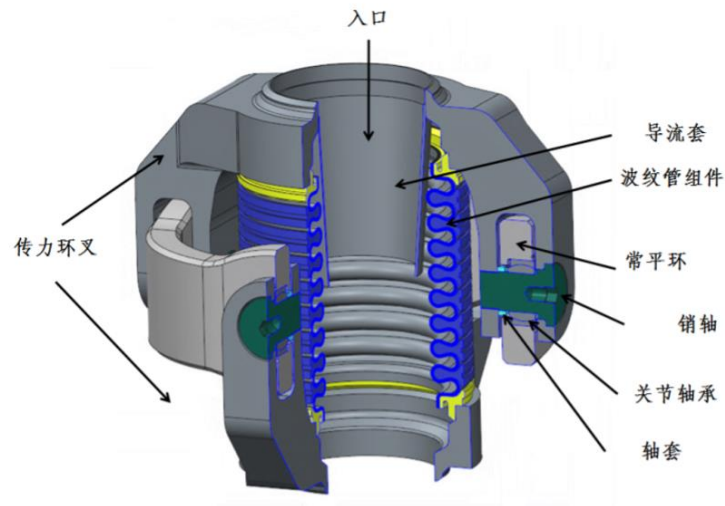


Fig. 1 The structure of the HPSC.

## 2.2 Finite Element Modeling

In consideration of the fact that multi-layer bellows operate within a range of large elastoplastic deformations during service, involving issues of material elastoplasticity and boundary contact nonlinearity, it is difficult to perform an integral simulation with the external load-bearing structure. Therefore, the HPSC is divided into the bellows assembly and the load-bearing structure for separate modeling.

The external load-bearing structure mainly withstands the medium separation force produced by internal pressure during operation. Consequently, the load-bearing structure is modeled using solid elements. The bellows mainly bear internal pressure and bending loads. Considering the geometric form of their structure and the symmetry of the bending loads, both two-dimensional and three-dimensional axisymmetric models are utilized for simulating the mechanical performance. The finite element model is shown in Figure 2.

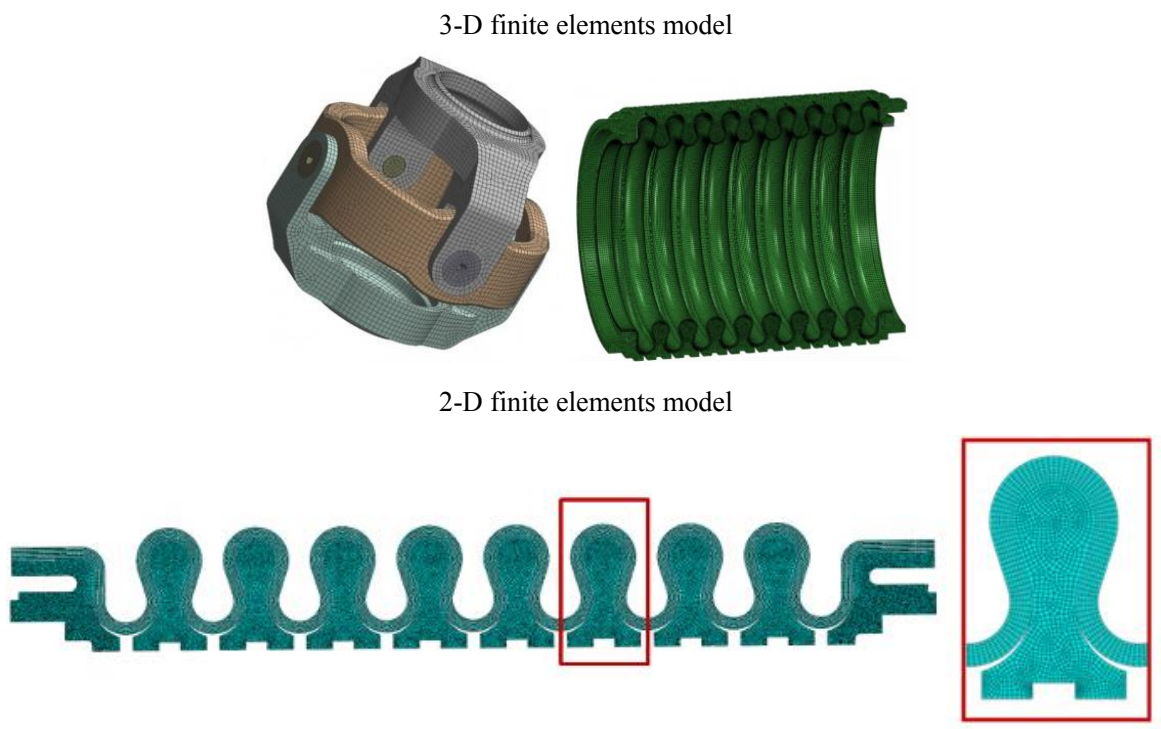


Fig. 2 Finite element models of the bellows and the load-bearing structure.

To simulate the actual contact conditions of the structure, Inner and outer rings of the bearing are set as a friction pair, with a friction coefficient of 0.08. The pin and the force-transmitting ring fork are connected via a threaded connection, which is simplified into a Tie constraint. Between each layer of bellows, as well as between the bellows and the interface ring and the armored ring, contact friction pairs are established. The contact type is set as surface-to-surface contact with a Finite Sliding type, and the friction coefficient is designated as 0.1.

### 3 Mechanical Performance Analysis

The HPSC is required to adapt to conical swinging. The structural stress situation is shown in Figure 3, and a mechanical performance analysis is conducted separately for the bellows assembly and the load-bearing structure.

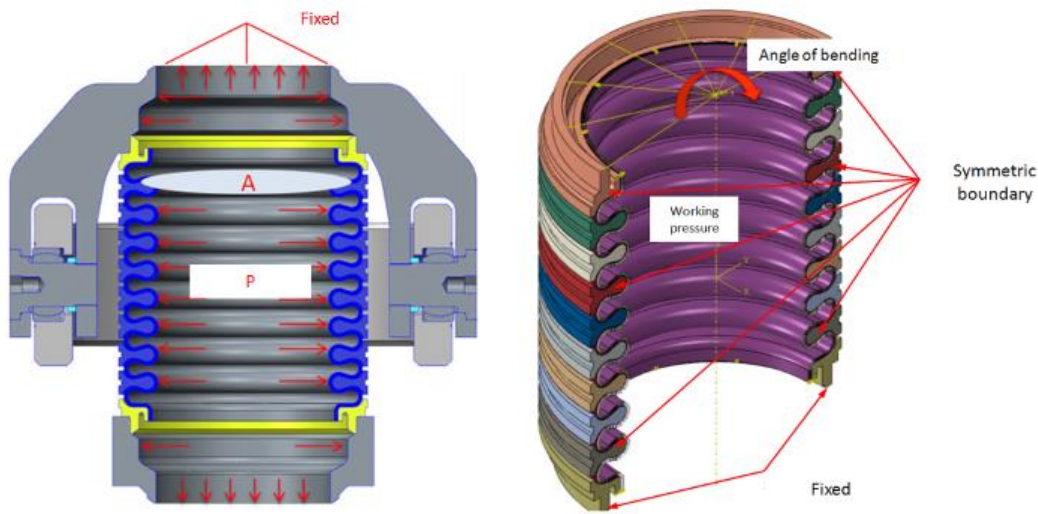


Fig. 3 Structural boundary and force condition of the HPSC.

#### 3.1 Strength Analysis

Taking into account the rotational friction contact, the calculations yield the Mises stress values for the external load-bearing structure in both the neutral position and during the swing state. Specific results can be found in Figure 4.

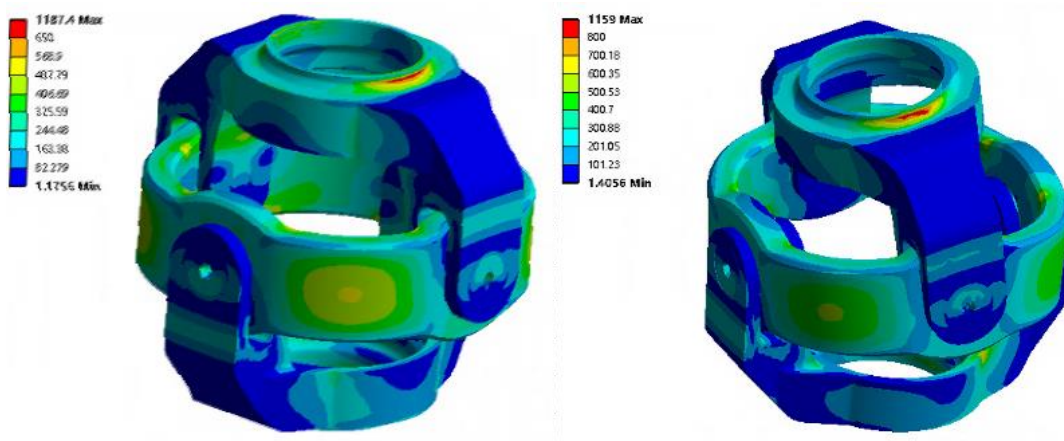


Fig. 4 Stress distribution diagram of the external load-bearing structure in the neutral position and during the swing state.

The stress level of the overall structure, except for the stress concentration caused by line contact, is less than the yield strength of the material, and it meets a safety margin of 1.5 times. Considering the contact nonlinearity brought about by the interaction between layers of the structure, the calculations provide the Mises stress values for the bellows in both the neutral position and during the swing state. Specific results can be found in Figure 5.

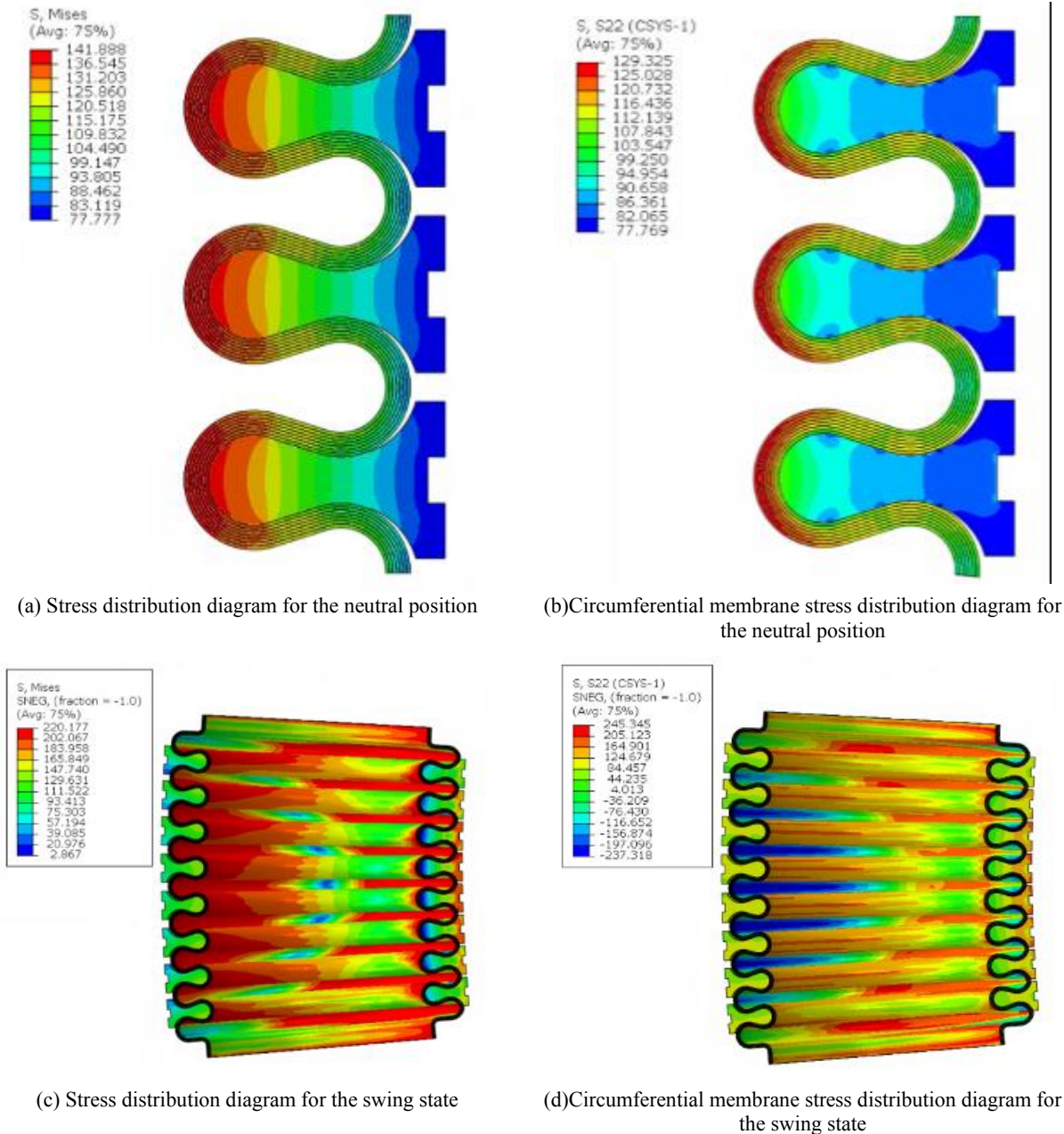


Fig. 5 Bellows Mises stress and circumferential stress distribution diagram.

From Figure 5, it can be seen that when the S-type armored bellows are subjected to internal pressure load, the maximum stress on the bellows is 141.9MPa, and the maximum circumferential membrane stress on the bellows is 129.3MPa. The Mises stress of the bellows is smaller near the crest of the wave and is generally higher on the inner layer than on the outer layer. The stress is larger at the trough position and the connection between the peak and the trough, with the maximum stress occurring at the trough. Therefore, the pressure-bearing capacity of the S-type armored bellows is mainly limited by the level of the Mises stress at the trough position.

Figure 6 shows the distribution of circumferential membrane stress for each layer of bellows along the meridional direction (from peak to trough to peak). The bellows layer closest to the armored ring is defined as the first layer. The theoretical values are based on the results calculated using the EJMA formula, and it can be observed that the distribution pattern of circumferential membrane stress is essentially the same for each bellows layer, with the average stress of the bellows close to the theoretical analysis results.

When the bellows are bent to  $8^\circ$  under a 20MPa load, the wave-shaped part of the bellows, particularly on the compressed side at the peak, experiences higher stress due to the squeeze from the armored ring, with the maximum circumferential stress being 245.345MPa.

### 3.2 Bending Stiffness Analysis

The bellows within the high-pressure swing device primarily serve to provide swing compensation functionality. Based on their actual working conditions, an analysis of their bending stiffness is conducted. Utilizing the numerical simulations, the reaction forces  $RF_x$ ,  $RF_y$ , and the reaction moment  $RM_z$  at the loading point are obtained. By considering the bending angle, the reaction forces are decomposed into two directions, yielding the transverse force  $F_v = RF_x \cos \alpha + RF_y \sin \alpha$  and axial force  $F_i = RF_x \sin \alpha + RF_y \cos \alpha$  experienced by the bellows during the bending process. The axial force does not produce a bending moment, as shown in Figure 7.

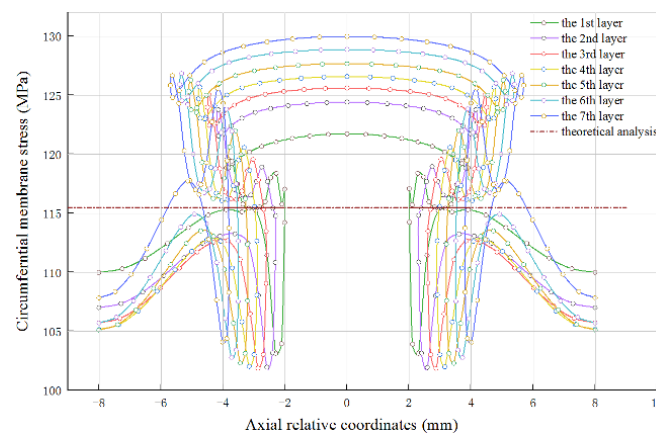


Fig. 6 Circumferential membrane stress curve diagram for each layer of bellows along the meridional direction.

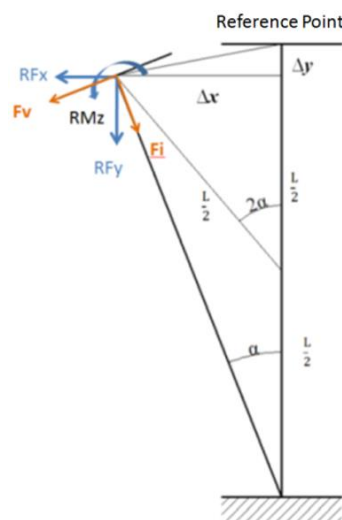


Fig. 7 Decomposition of loads during the bellows bending process.

Therefore, the bending moment  $M$  of the bellows is the superposition of the bending moment produced by the transverse force and the reaction moment. The formula is as follows:

$$M = RM_z + F_v L \quad (1)$$

Figure 8 shows the curve of the bending angle versus bending moment for the bellows. It can be observed that in the 0-1.6° phase, the angle-moment curve of the bellows is linear. When the S-type armored bellows are bent to 3°, the bending stiffness of the bellows decreases slightly, primarily due to the structure entering the plastic phase locally, which leads to a reduction in the bending stiffness of the bellows; when bent under load to 6°, the bending stiffness of the bellows suddenly increases, mainly because the crests of the bellows and the strengthening rings are fully in contact, resulting in an increase in bending stiffness. The bellows exhibit significant non-linear characteristics during the bending deformation process, with the bending stiffness of the structure being affected by the non-linearity of the bellows material and the degree of contact of the local structure. From the swinging process of the bellows, it can be seen that the local structure of the bellows enters plastic yielding, which has a noticeable impact on the structural strength and fatigue life.

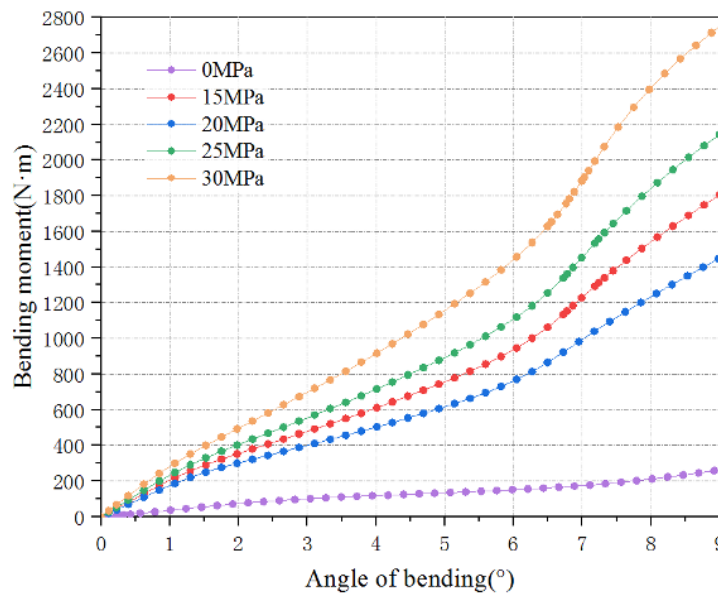


Fig. 8 Curve diagram of angle versus bending moment under a 20MPa bending load.

## 4 Low Cycle Fatigue Life Analysis

### 4.1 Analysis Method

In the process of reciprocal bending, the bellows experience substantial local plastic yielding, which falls under the category of low-cycle fatigue. The Goodman method is used to superimpose calculations for fatigue life. Due to the local plastic deformations of the bellows, a modified Manson-Coffin formula (strain-life curve) is employed to estimate the fatigue life, as shown in Equation 2.

$$\frac{\Delta \varepsilon_a}{2} = \frac{\Delta \varepsilon_e}{2} + \frac{\Delta \varepsilon_p}{2} = \frac{\sigma_f'}{E} (2N_f)^b + \varepsilon_f' (2N_f)^c \quad (2)$$

During the short-life phase, where the plastic strain range  $\Delta \varepsilon_p$  is predominant and the elastic strain range  $\Delta \varepsilon_e$  can be neglected, the strain fatigue calculation formula can be further simplified to the following expression:

$$\frac{\Delta \varepsilon_p}{2} = \varepsilon'_f (2N_f)^c \quad (3)$$

Where  $\varepsilon'_f$  is the fatigue ductility coefficient, which is approximately equal to the true strain at the breaking point of the material during static tensile testing;  $c$  is the fatigue ductility exponent. Further considering the load asymmetry, the average strain  $\varepsilon_m$  is introduced for correction, resulting in the modified fatigue life calculation formula as Equation 4.

$$\frac{\Delta \varepsilon_p}{2} = \varepsilon'_f \left(1 - \frac{\varepsilon_m}{\varepsilon_b}\right) (2N_f)^c \quad (4)$$

Where  $\varepsilon_b$  is the strain corresponding to the local stress of the structure reaching the strength limit, which is approximately equal to  $\varepsilon'_f$ .

#### 4.2 Fatigue Calculation Results

Under bending load, when bent to 8 degrees, the equivalent plastic strain (PEEQ) contour map of the S-shaped bellows is as shown in Figure 9. PEEQ  $\geq 0$  indicates that the material has yielded. It can be observed that the maximum plastic strain occurs near the armor ring at the wave crest. The local material of the bellows enters the yield strength; therefore, the bellows will undergo low-cycle fatigue. The plastic strain value at the wave crest position is 0.03, which establishes that this location may be the potential point of fatigue failure.

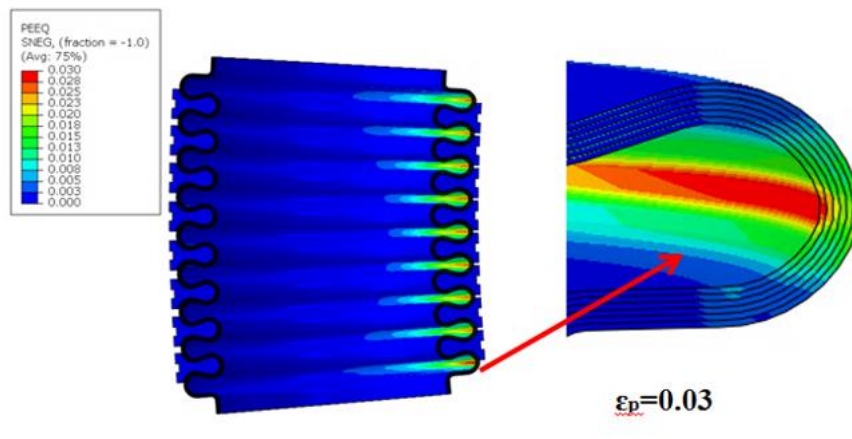


Fig. 9 Bellows Equivalent Plastic Strain Distribution.

At the critical point, the single direction's maximum strain value is 0.03, and under the combined effect of the average stress caused by internal pressure, using Equation 2, the median fatigue life of the hose is calculated to be 3357 cycles. Based on the strain-corrected Manson-Coffin formula, the fatigue life assessment method can reflect the structural mechanical properties more accurately.

### 5 High-Pressure Swinging Experiment

#### 5.1 Experiment Setup

According to the actual operating points of the HPSC, to fully verify the static strength characteristics and swinging operational characteristics of the swing component, the tests include two conditions: high-pressure swing tests and fatigue life tests. The inlet and outlet ends of the HPSC are fixed on the test bench's fixed beam and the actuator cylinder, respectively, through bolt connections. By measuring and adjusting the vertical height

of the actuator cylinder and the axial perpendicularity to the swing component, the zero position of the servo mechanism during the swing process is ensured to be consistent with the zero position of the swing component. The test measurements mainly involve the bending stiffness of the swing device and the structural strain.

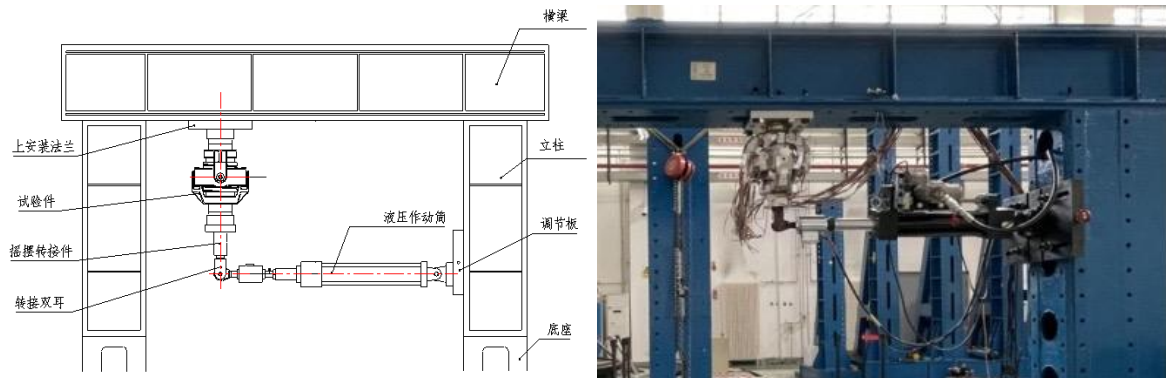


Fig. 10 Experimental system structure and physical object.

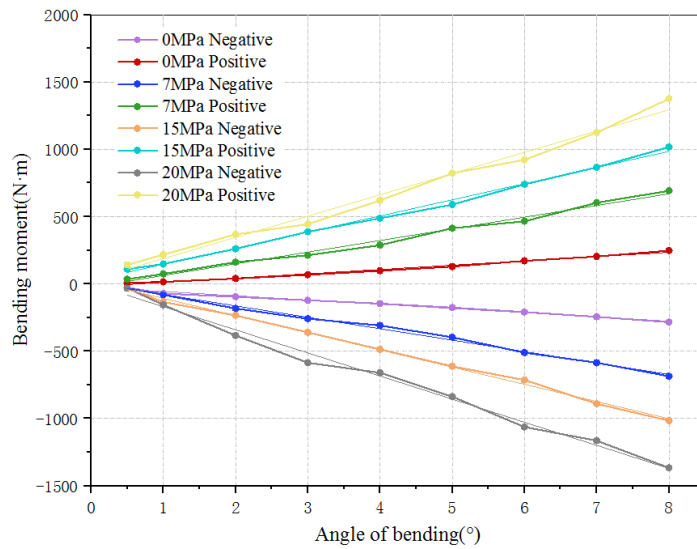


Fig. 11 The measured moments of the HPSC in the experiment.

## 5.2 Test Results

**Swinging Moment** Through the experiment, the corrected torque of the HPSC was obtained under different pressures  $p = 0, 7, 15, 20\text{MPa}$  and swing angles  $a = 0.5, 1, 2, 3, 4, 5, 6, 7, 8^\circ$  in the swing tests. The relationship between swing torque and angle variation is shown in Figure 11.

The test data curves clearly show a linear trend. The curves are subjected to linear regression analysis, and during this fitting process, there are no unused invalid values. Table 2 shows the angle- swing torque linear regression results. The coefficient of determination,  $R^2$ , can effectively reflect the overall fit of the regression equation; the closer the  $R^2$  value is to 1, the better the fit. From the fitted data, it can be seen that the coefficient of determination  $R^2$  for all 10 sets of data is greater than 0.99, indicating that each set of data has a good overall fit. All curves are fitted in the form of  $ax + b$ . Analysis of the experimental data shows that, under various angles and pressures, the positive and negative swing torques are essentially consistent; the swing torque at each pressure level increases with the angle, following a relatively stable upward trend, and the data exhibits good follow-through and consistency.

Table 2 Angle-swing torque linear regression results.

Condition	Slope/a	Intercept/b	R <sup>2</sup>	PR
0MPa Negative	-31.39	-25.33745	0.99014	-0.99456
0MPa Positive	-31.39625	-20.63241	0.99018	0.99508
7MPa Negative	-31.93676	6.83696	0.99552	-0.99776
7MPa Positive	-84.8913	-24.01433	0.99013	0.99505
15MPa Negative	86.66107	20.20504	0.99733	-0.99866
15MPa Positive	-127.667	25.51186	0.99595	0.99797
20MPa Negative	119.90119	2.18281	0.99191	-0.99594
20MPa Positive	-171.60672	29.72678	0.99053	0.99375

**Stress and Strain Data** During the pressurization process to 20MPa, the strain curves for some of the measuring points are shown in Figure 12. The maximum strain occurs at measuring point s8, reaching 1564  $\mu\epsilon$ , corresponding to a unidirectional stress of 312.7MPa, which did not reach the yield limit of the material. The strain data from the experiments indicate that the maximum stress value at the structural location of interest did not reach the material’s yield strength. There was no significant deformation in the overall structure during the testing process. During the fatigue swinging process, the stress level remains stable without any sudden stress changes.

**Fatigue Life Test** During the fatigue life test, under high pressure and swing frequency conditions ranging from 0.1 to 2Hz, the number of swing cycles exceeded 3000, meeting the requirements for fatigue life. After multiple swings during the fatigue life test, the swing torque increased significantly, with the maximum torque reaching 2133Nm. The primary reason for this increase is attributed to wear between the inner and outer rings of the joint bearings due to repeated swinging, and inadequate lubrication leading to increased friction torque.

### 5.3 Simulation and Experimental Result Error Analysis

To validate the effectiveness of the simulation method used in this paper, the swing torque is compared with the strain measurements at structural points. The swing torque of the HPSC is primarily due to the bending moment of the bellows. To assess the accuracy of the bellows simulation modeling, the bending moment obtained from the simulation of the swing device’s bellows is compared with the torque gathered from the experiment.

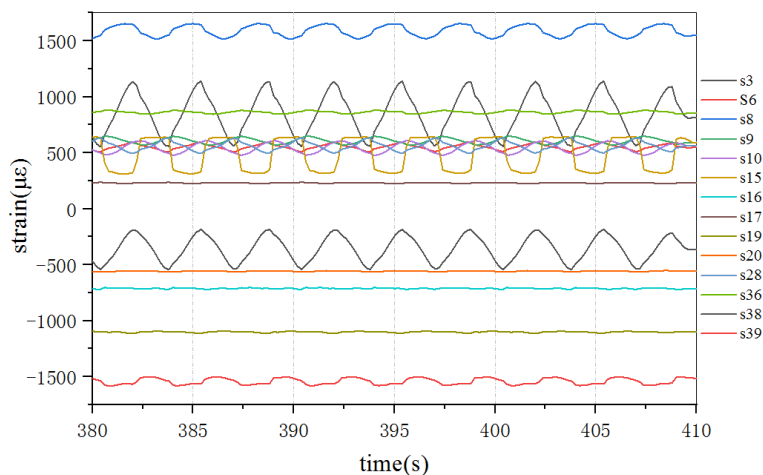


Fig. 12 The multi-point strain curves of HPSC gathered from the experiment.

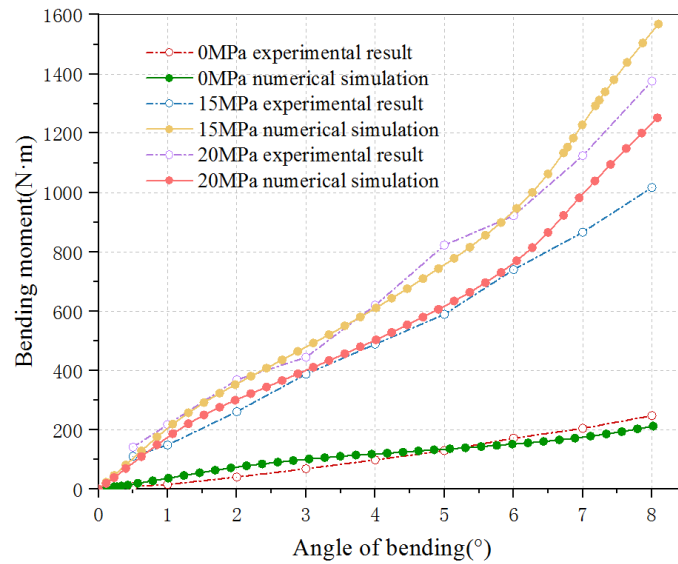


Fig. 13 HPSC swing torque simulation and experimental results comparison curve.

From Figure 13, it can be concluded that the trend of the simulation results is generally consistent with that of the experimental results. The torque curves almost coincide when there is no load, and the error between finite element simulation results and experimental data is at most 5% within a 6° swing angle. The error tends to be larger within the 6-8° swing angle range. Analysis suggests that in the finite element simulation, the deformation of each corrugation of the bellows is more significant near the upper and lower end surfaces. When the bellows undergo large-angle deformation, the bellows completely adhere to the reinforcement ring, causing a sharp increase in bending torque.

The actual deformation and fitting situation deviates from the finite element simulation to a certain extent, and this discrepancy significantly affects the bending torque under large-angle deformation. The strain measurements at key points of the swing device structure are compared with the maximum unidirectional stress values extracted from the corresponding points in the simulation model. The results are shown in Figure 14.

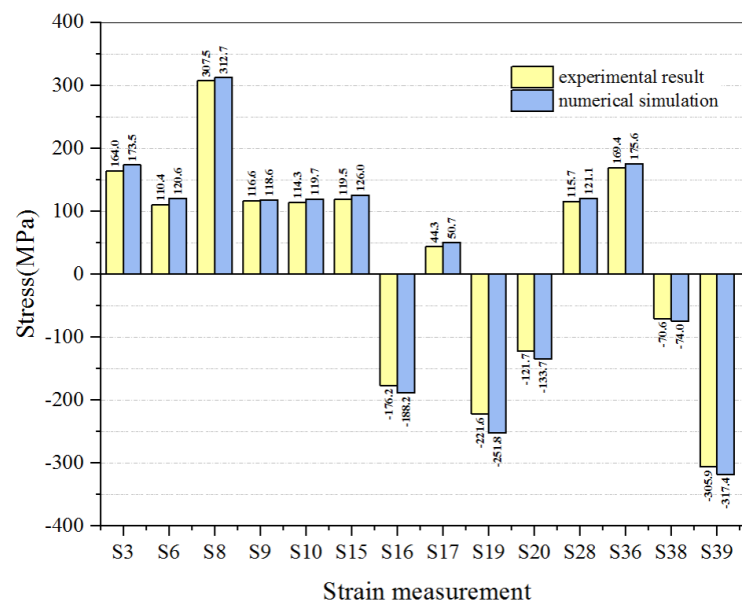


Fig. 14 Comparison of simulation and measurement results of load-bearing device structural stress. The maximum error between finite element simulation results and experimental results is 15%.

The simulation and measurement have obtained good consistency for the stress at the measuring point positions, indicating that numerical analysis methods are able to accurately capture the stress levels within the structure.

## 6 Conclusion

Through mechanical performance analysis and experimental research on a HPSC for a SAP engine, a finite element model was established, simulated under actual working conditions, and the product was subjected to high-pressure swing tests. Simulation results were compared with experimental measurements, and the test results were analyzed in detail. This research shows:

(1) The paper adopted mixed element modeling for simulating the swing component, and the structural stresses matched well with the experimental results, indicating that the finite element simulation could essentially reflect the structural stress state.

(2) The bending torque of the bellows exhibited nonlinearity with varying loads. At small angles, the material remained in the linear-elastic stage, with high structural compression and bending stiffness. As the load increased to a certain level, the material yielded, and the structural stiffness began to decrease. With further increased loading, the peaks of the bellows adhered to the reinforcement ring, and the stiffness showed a significant increase again.

(3) The consistency between the experimental data and the simulated torque results of the high-pressure swing device is good, which validates that the simulated stiffness of the bellows can effectively mimic the actual stiffness of the product.

(4) A fatigue life analysis method for the swing device based on the strain-corrected Manson-Coffin formula was proposed. The fatigue life evaluation method can reflect the structural mechanical properties more authentically and provide optimization direction for life prediction under complex working conditions.

(5) The main factor influencing the swing torque of the HPSC is the bending torque of the bellows. After the fatigue swinging test, the increase in swing torque is primarily due to the increased friction torque of the bearings.

(6) The experiment effectively simulated the actual operational boundaries and test conditions, effectively verifying the strength characteristics of the HPSC during the swinging process, assessing its fatigue life, and acquiring the actual swing torque. This provides significant experimental data for the development of SAP engines.

## References:

- [1] Anderson, W.: Analysis of stresses in bellows. part i. design criteria and test results. Tech. rep., Atomics International. Div. of North American Aviation, Inc., Canoga Park (1964)
- [2] Bin Li, Zhanguo Liu, F.I.L.G.M.Z.: Research on key technologies of 130-ten pump rear swing high-pressure staged combustion lox/kerosene engine. *Manned Spaceflight* 28(433-438) (2022)
- [3] Eckard, T.: Liquid rocket lines, bellows. flexible hoses, and filters. NASA space vehicle design criteria, NASA SP-8123 (1978)
- [4] Lang, Z.: Mechanical Properties Analysis of Multi-Layer S-type Bellows. Master's thesis, Dalian University of Technology (2012)

- 
- [5] Morgan, P., Saunders, A., Rajah, M.: The measurement of pressure drop in fluid flow. *The Engineer* (London, England) 214, 359-360 (1962)
  - [6] Shawket, A.: The Dynamic Performance Analysis and Structural Parameter Optimization of S-shaped Welded Metal Bellows. Master's thesis, Xinjiang University (2012)
  - [7] TM, Hulbert, L., Lestingi, J., Keith, R., LABS, B.M.I.C.O.C.: Development of analytical techniques for bellows and diaphragm design. Battelle Memorial Institute AFRPL TR 68, 22 (1968)
  - [8] Weijing Wang, Yuqiang Yang, S.Y.Z.L.: Study on fatigue life of u-shaped bellows under displacement load. *Pressure Vessel Technology* 39(63-68) (2022)
  - [9] Yuan, Z.: Study on Mechanical Properties of S-shaped Bellows Reinforced by Hydraulic Forming. Ph.D. thesis, Northwestern Polytechnical University (2019)
  - [10] Zhou, Z.: Stiffness and Fatigue Life Analysis of Bellows Assembly for Aerospace Gas Valves. Master's thesis, Beijing Institute of Technology (2015)